Proceedings of the 12th International Conference on Fluid Flow, Heat and Mass Transfer (FFHMT 2025)
July 15, 2025 - July 17, 2025 | Imperial College London Conference, London, United Kingdom
Paper No. 171
DOI: 10.11159/ffhmt25.171

Computational Study of Melting and Solidification in a Prototype Four-pass Thermal Storage Module

Luca Crnjac[1], Kamran Siddiqui[1], Anthony Straatman[1]
[1]Western University
1151 Richmond Street, London, Canada
lcrnjac@uwo.ca; ksiddiq@uwo.ca; agstraat@uwo.ca

Abstract – A computational study is presented that utilizes the enthalpy-porosity model in ANSYS-Fluent to predict melting and solidification for the base case of a simple four-pass thermal storage module containing a paraffin phase change material. The prototype module is a rectangular prism of square cross-section oriented vertically with four stainless steel tubes passing through it for passage of a heat transfer fluid (HTF). The computational model was calibrated in a previous study and was utilized with the properties provided for the PCM. Comparisons between the computed results and experimental results reported previously for the same module show that the enthalpy-porosity model predicts the flow, the interface structure and the melting time reasonably well. The same model predicts the evolution of the interface structure during solidification reasonably well but over-predicts the solidification time by more than double. This implies that calibration must be done for both processes to capture the impacts of the different interface structure and the impact that temperature gradient and interface evolution have on processes and thermophysical properties. Comparisons of the outlet temperatures during melting were also reasonably well predicted in terms of trend and value. In its current form, the model is useful for the development of heat transfer elements that consider enhancements to shorten charging (melting) times of the module. The results of this study are a baseline from which enhancements in terms of HTF flowrate and heat transfer elements can be compared.

***Keywords*:** Thermal Storage, Phase-change Materials, Computational Modelling

1. Introduction

Thermal Energy Storage (TES) is the concept of storing and accumulating available thermal energy such that it can be utilized when needed for heating processes [1]. This can be accomplished by capturing solar/waste heat when available to increase the thermal energy of a storage medium and then recovering the energy when it is required for secondary heating processes like, for example, residential space and water heating. This technology makes it possible to better utilize intermittent resources like solar energy for heating, thereby reducing our dependency on conventional non-renewable energy sources like fossil fuels. When implemented in a modern energy system, TES has the potential of an increase in overall efficiency, better reliability, better economics, and less pollution to the environment [2].

TES can be generally subdivided into two categories: sensible heat storage, and latent heat storage. These two types of storage are associated with different parts of a standard heating curve for a material that can exist in multiple phases. Sensible storage refers to storage under a uniform phase (solid, liquid or vapor) and results in a temperature change of the medium, the level of which is dictated by the specific heat capacity of the energy storage material and the phase in which storage is occurring. Given the low specific heat capacities of common solids, liquids and gases, significant storage is only possible when very high temperatures are achieved. Latent storage refers to the storage in a medium undergoing a phase change from solid ↔ liquid or liquid ↔ vapor. In these cases, large amounts of energy can be absorbed or released at a near-constant temperature wherein the amount of storage is dictated by the fusion or vaporization enthalpy of the medium. For thermal storage vessels designed to maximize energy storage, solid ↔ liquid storage has numerous advantages including (but not limited to): high latent heat of fusion, near-constant temperature during phase change and low volumetric expansion between phases. In addition, there are many low-cost phase change material (PCM) alternatives that change phase at temperatures in the range 30-70^{o}C range which is both safe and effective for residential space and water heating.

When utilized in solid ↔ liquid latent TES systems, common energy storage materials like, for example, paraffins or sodium acetate trihydrates (SATs) have energy storage densities that are 50-100 times higher than sensible heat systems,

however these media have very low conductivity, which can make charging (melting) and discharging (solidification) processes slow. While significant research has been conducted to understand the heat transfer processes that occur during melting and solidification ([4-5], for example), further effort is required to transfer this knowledge into the design of TES vessels that can be charged quickly and uniformly and discharged at rates that are suitable for the specific heating application. Extensive experiments have been conducted on different shaped enclosures [4,6,7] to understand fundamental heat transfer processes and these studies have been used to calibrate computational models [8,9] that can be used in the development of individual cells of a multi-cell TES vessel. What is clear from these studies is that heat transfer during charging and discharging has both conductive and convective components, the balance of which depends on the thermophysical properties of the PCM and the size, shape and orientation of the vessel. In addition, because a phase change is occurring, the relative amounts of solid/liquid in the vessel (and, consequently, the apparent shape of the liquid region) is constantly changing making the process inherently transient. As such, exploitation of the inherent heat transfer processes to shorten charging and discharging times requires an understanding of these processes in the vessel under consideration.

The current study is a small part of a larger effort focused on the development of a multi-cell TES vessel that can be utilized in residential space and water heating. The present study describes computational modelling of a 4-pass prototype thermal module with comparison to similar experiments conducted previously for the purpose of providing a baseline from which to develop heat exchanger elements to shorten charging and discharging times.

2. Computational Approach

Many algorithms and methods have been developed for conducting simulations of melting and solidification. The most popular commercial software products used for detailed computational fluid dynamics (CFD) studies include COMSOL and ANSYS Fluent. COMSOL is a commercial CFD software which employs the apparent heat capacity method for solving melting and solidification cases. This method captures the phase change interphase implicitly by solving the heat transfer equation with effective material properties for both phases. The latent heat capacity is accounted for by modification of the material heat capacity [9]. ANSYS Fluent utilizes the enthalpy-porosity method [11] in which the solid-liquid interface is not explicitly tracked, but rather the mushy zone separating the solid-liquid region is treated as a "pseudo" porous medium. Many studies have been conducted using this method and show good agreement with experimental results [12-14]. Computations for the present work have been undertaken using ANSYS Fluent and compared to experimental results presented in [15]. The mass and momentum equations for thermal behaviour and phase change of a PCM are given in the ANSYS Fluent manual as [11]:

$$\nabla \cdot \vec{V} = 0 \tag{1}$$

$$\rho\left(\frac{d\vec{V}}{dt} + \nabla \cdot \left(\vec{V}\vec{V}\right)\right) = -\nabla P + \nabla \cdot \left(\mu \nabla \vec{V}\right) - \rho \vec{g} c_i \alpha \left(T - T_{ref}\right) + \vec{S}_m \tag{2}$$

where $\vec{V}$ indicates the vector of velocity (m/s), ρ is the density of the PCM (kg/m^3), t is time (s), μ is the dynamic viscosity $(kg/m\,s)$, P is the kinematic pressure (Pa) , $\vec{g}$ is the acceleration due to gravity (m/s^2), T is temperature (K), T_{ref} is the reference temperature (K) in the buoyancy source term, $c_i\alpha$ is the buoyancy parameter comprised of the thermal expansion coefficient α $(1/K)$ and a convective intensity coefficient c_i, and $\vec{S}_m$ is a mushy-zone source term. The convective intensity coefficient is added as a control parameter that can be used to account for the aggregate effect of influences that are not modelled specifically, e.g. the impact of temperature on material properties [16]. The mushy-zone term slows the fluid velocity in the mushy region where the liquid fraction (or porosity) ranges between 0-1, and is defined as:

$$\vec{S}_m = \lambda \vec{V} = \frac{(1-f)^2}{f^3 + \varepsilon} A_{mush} \vec{V} \tag{3}$$

Here, A_{mush} is the mushy zone coefficient $(kg\ m^{-3}s^{-1})$, f is the liquid fraction defined in Fluent as a function of temperature, and ε is a small number to avoid division by zero (0.001 in ANSYS Fluent [11]).

The energy equation is given as:

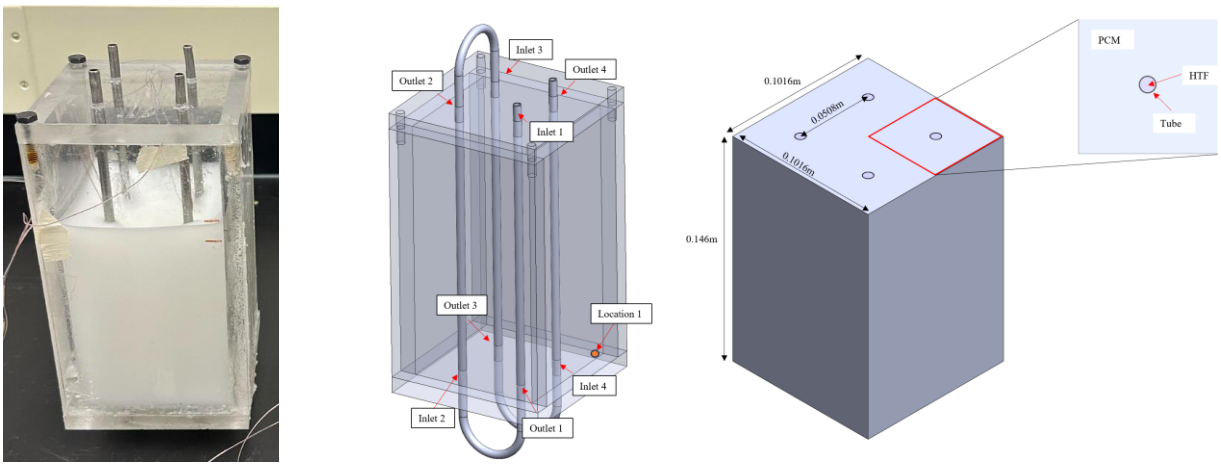

Fig. 1: Images showing the physical thermal module prototype (left), the CAD analogy (center), and the computational domain (right), which only includes the portion of the physical prototype filled with PCM.

$$\frac{\partial}{\partial t}(\rho H) + \nabla \cdot \left(\rho \vec{V} H\right) = \nabla \cdot (\mathrm{k}\nabla T) + S_E \tag{4}$$

where k is thermal conductivity (W/m K) and S_E is a source term that can be applied to capture reactive effects ($S_E = 0$ in this work). The sum of the sensible enthalpy ($h\,[J/kg]$) and the latent heat content ($\Delta H\,[J/kg]$) is used to compute the enthalpy of the materials during the phase change process as:

$$H = h + \Delta H \tag{5}$$

where $\Delta H = f L_H$ and L_H is the latent heat of fusion (J/kg).

In terms of computational setup, the pressure-based solver in ANSYS Fluent was selected for both melting and solidification simulations. Gravity was enabled to allow for buoyancy-driven natural convection to occur in the PCM, and the SIMPLE algorithm was used for pressure–velocity coupling. The PRESTO! algorithm was used for pressure discretization as it is recommended for natural convection; and second-order schemes were used wherever possible for modelling advection. The only exception is the momentum equation which utilized first-order advection to avoid numerical instabilities. The mushy zone coefficient was set to A_{mush}= 3×10^5 and the convective intensity coefficient was set to give $c_i\alpha$= 0.0004 (see Eq. 2) based on a calibration study comparing experimental and simulated melting times (see Crnjac [15]).

The geometric model of the 4-pass TES prototype is shown in Fig. 1. The vessel has a square cross-section of 0.1016 m and height 0.1460 m with tubes passing through vertically in the arrangement shown in Fig. 1. The tubes are stainless steel with an outside diameter of 6.35 mm and wall thickness 0.25 mm. During experimentation, the vessel and the tubes extending out of the vessel were heavily insulated using insulation blankets to mitigate heat losses [15], but some stray heat transfer losses were unavoidable because of the high temperature of the working fluid and the process times. The portion of the full domain that was modelled computationally is shown in the right image in Fig. 1, which only includes the PCM volume inside the vessel, the tubes and the working fluid inside the tubes. The airspace above the PCM was not modelled, nor were the short loops connecting the tube passes for the working fluid. The tubes and the PCM region were discretized using hexahedral cells in an unstructured grid arrangement, and grid density was determined from a calibration study reported in [15].

Adiabatic boundary conditions were imposed on all external surfaces of the PCM domain, while the interfaces between the PCM and the tubes were thermally coupled. The heat transfer fluid (HTF) for both heating (melting) and cooling (solidification) entered *Inlet* 1 and after 4 passes, exited from *Outlet* 4. As only the domain inside the module was discretized (Fig. 1b), temperature/flow information throughout the transient simulation was simply transferred from the *Outlet* of one tube to the *Inlet* of the next based on the assumption that the short, flexible (rubber) loops connecting the passes through the module were adiabatic. Computations were run using a 1-second timestep until the PCM domain was fully melted (or

Tab. 1: Thermophysical properties of Polyfin PCM at 25°C [4].

Property [units]	Value
Melting temp [°C]	55
Density, ρ [kg/m^3]	920
Specific Heat, C_P [kJ/kg K]	2.89
Thermal Conductivity, k [W/m K]	0.18
Dynamic Viscosity, μ [kg/m s]	0.00506
Thermal Expansion, α [1/K]	0.00058
Heat storage capacity, L_H [kJ/kg]	180

solidified), which was monitored by consideration of the liquid fraction or specific temperature markers. Thermophysical properties of the PCM used in the experiments are given in Tab. 1. The material is commercially available as Polyfin [4].

3. Results and Discussion

Computations on the domain shown in Fig. 1 (right) lead to complete three-dimensional, transient results of melt fraction [15], images of the solid-liquid interface, and temperature data for all points inside the PCM domain and at the inlet and outlet of each tube pass. Two thermocouple locations were used to monitor the start and end of a charging/discharging event during the experiments [15]: one located at the geometric centre of the PCM domain 0.0508m off each vertical wall and 0.073m off the base (hereinafter called TCC); and one located near a lower corner of the PCM (Location 1), as indicated in Fig. 1.

3.1 Charging

The charging (melting) experiment used in this comparison started with the initial condition of T_{PCM} = 23°C. Water at constant temperature of 80°C was provided at *Inlet* 1 at a mass flow rate of $\dot{m}$ =0.20 kg/min (Re_d= 720) until the thermocouple at Location 1 reached 60°C, which is above the liquidus temperature of 55°C (the lowest temperature at which the PCM is completely liquid). This required a total melting time of 25,073 s (6.96 hours). The computations had the identical initial condition and predicted a total melting time of 23,916 s, which is 4.6% longer. An additional comparison was made between the measured and computed energy consumption required to produce the phase change and temperature rise. The experimental energy consumption was calculated by monitoring the inlet and outlet temperatures of the HTF and then integrating $\dot{m}C_P\Delta T(t)\Delta t$ over the time of the experiment, where $\Delta T(t)$ is the instantaneous temperature difference between the inlet and outlet of the HTF and Δt is the time interval between temperature measurements, which also serves as the time step in the (discrete) integration operation. The energy consumption computed from the temperature measurements was 550 kJ compared to 442 kJ predicted using the CFD model. The difference between the experimental and computed results are reasonably attributed to heat losses in the experiment that are not accounted for computationally. Given the difference in absolute melting times, results of melt fraction and temperature are presented using the dimensionless timescale $\tau+ = t/t_{tot}$, where t is the actual time into the melt and t_{tot} is the total melting time. Figure 2 compares simulated melt fraction contours extracted along a plane that passes through two HTF tubes to experimental images of the melt fraction at various dimensionless times. The figure shows qualitatively good agreement between the simulated and experimental melt fractions at each dimensionless time.

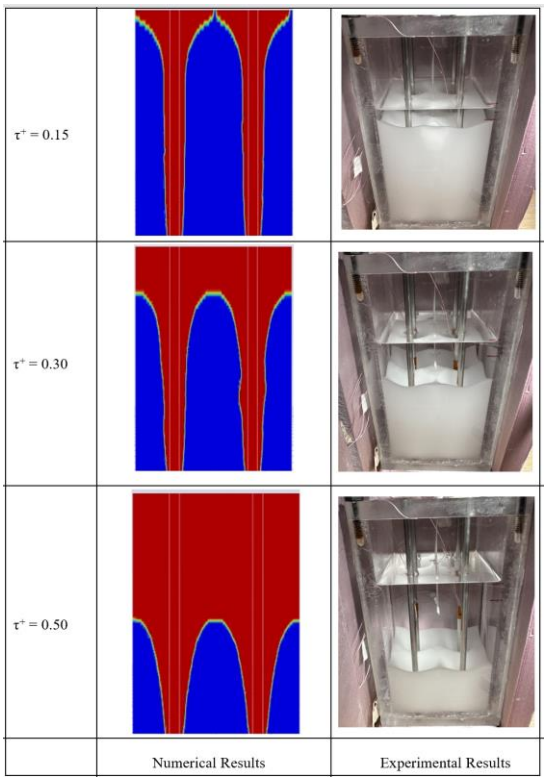

Fig. 2: Comparison of simulated and experimental melt fraction contours at three dimensionless times. Numerical results are presented for a vertical plane that cuts through two HTF tubes, wherein red indicates liquid and blue denotes solid PCM.

Melting is observed to start at the tube surfaces where the melted liquid rises along each tube until it reaches the surface. To satisfy mass, liquid is drawn inward towards the tube and down the annular pocket at the liquid-solid interface around the tube, which causes the pockets to grow in an inverted toroidal cone pattern. As time progresses, the pockets enlarge and the liquid region at the PCM surface continues to grow to the point where no more solid PCM exists in the module, which is the instant when Location 1 reaches 60°C. Figure 3 compares the time evolution of the HTF temperature at *Inlet* 1 and *Outlet* 4 of the module for the experimental and computational cases in real time. The plot shows that there is good agreement between the fluid temperatures in the initial stages of the melting process, but the computational model over-predicts the outlet temperature beyond 8000 seconds, leading to lower overall heat transfer. The total heat transfer to achieve melting and warming is underpredicted by the computational model by 20%, but as noted above, this can be reasonably attributed to heat losses that are not accounted for in the computations.

3.2 Discharging

The solidification (discharging) experiment was initiated from the condition at the end of the charging experiment, i.e. thermocouple Location 1 at 60°C. Water at constant temperature of 10°C was then provided at *Inlet* 1 at a mass flow rate of $\dot{m} = 0.20$ kg/min ($Re_d = 720$) until the thermocouple at TCC reached 50°C, which is below the solidus temperature (the highest temperature at which the PCM is completely solid). This required a total time of 9584s (2.7 hours). The computations had the same initial condition but predicted a solidification time of 19939s (5.54 hours), which is more than double the time established in the experiment. This suggests that the calibration parameters used for melting simulations are not suitable for simulations of solidification. The reduced temperature gradient and the evolution of the interface from solid to fluid during the solidification process impacts the interface structure and other property dependencies that may have a higher impact during solidification. A study by Yang et al. [8] shows detailed images of the interface during melting and solidification of a paraffin material and describes the interface as dissolving "flocs" during melting and thickening dendrites during

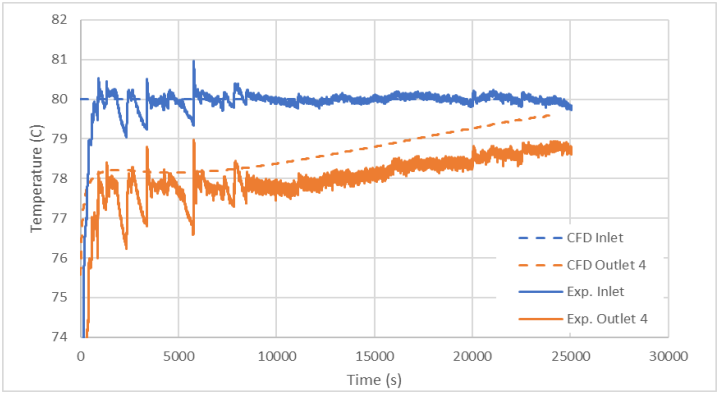

Fig. 3: Comparison between computational and experimental HTF temperature at the main Inlet and Outlet 4 of the TES module during melting.

solidification. The interface also appears in [8] to be thicker during solidification, which could be accounted for computationally by having different solidus and liquidus temperatures thereby permitting the mushy zone source term to be active in a larger region.

Scaling the process using the dimensionless time $\tau+$ still permits qualitative comparison to judge whether the CFD model predicts the main features of the process. Images of the liquid fraction for the computation and experiment are given in Fig. 4 for three instants in dimensionless time $\tau+$ on the same plane as indicated in Fig. 2 where it is observed that the solidification behaviour is reasonably well-predicted in terms of the evolving interface structure. In this case, solidification initiates on the tube walls causing liquid PCM to cool and drop along the growing layer of solid PCM. This reverse convection draws warm liquid PCM towards the tubes thereby slowing the solidification process at the top and producing the tall, inverted (solid) cone shapes around the tubes. The "flare" that forms at the top of these inverted cones at PCM surface is a result of the gradual turning of the warm liquid PCM as it is drawn down along the solid-liquid interface. While present, the flare shape predicted in the simulation is much more subtle likely due to the fact that surface effects and surface cooling were not included in the simulation.

3.2 Discussion

The comparisons of computed and experimental results for charging and discharging of a small, prototype thermal storage module show promise in terms of predicting the evolution of the interface shape during the heat transfer processes. The model used, which was calibrated for melting [15], does not do well for predictions of solidification time, which implies that the enthalpy-porosity model must be calibrated differently for melting and solidification. The main difference in terms of process is the magnitude of the thermal gradient and the evolution of the interface, which is from liquid to solid during melting and solid to liquid during solidification. This reversal in interface evolution causes differences in the interface structure and its thickness [8] and may also produce important property sensitivities to temperature which require attention in computational modelling. Future computational work is directed at calibration of the solidification model and consideration of other effects like supercooling. In terms of the 4-pass TES module itself, both the charging and discharging times for the baseline case are impractically long (based on experiments [15]) and require significant enhancement to be useful. Continued work on the module includes the addition of a metal honeycomb material and consideration of two types of metal wool to enhance heat transfer.

4. Summary

Computations are presented and compared to similar results of melting and solidification of a PCM in a prototype 4-pass TES module. The results show that the enthalpy-porosity model calibrated against melting experiments predicts both the structure and melting time reasonably well. Use of the same model for simulations of solidification show that

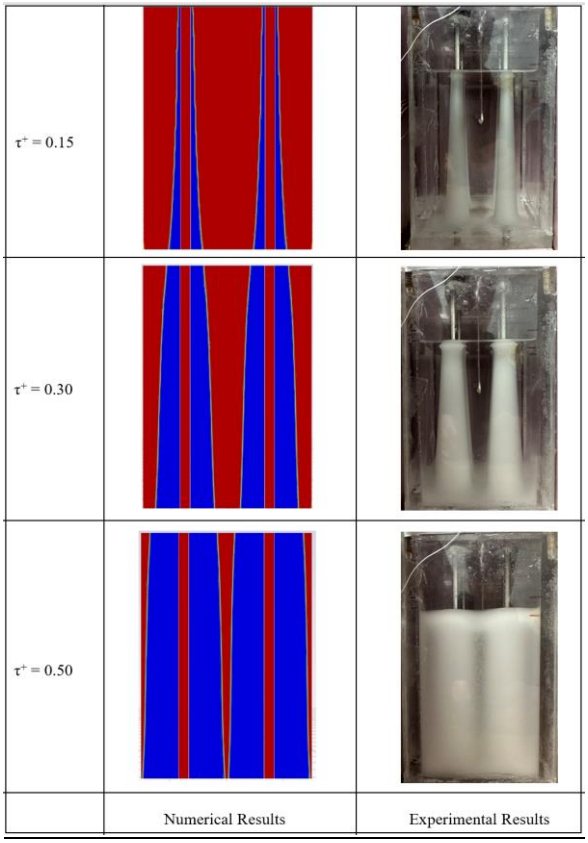

Fig. 4: Comparison of simulated and experimental melt fraction contours at various dimensionless times. Numerical results are presented for a vertical plane that cuts through two HTF tubes, wherein red indicates liquid and blue denotes solid PCM.

while the structure and shape of the solidification front are reasonably well-predicted, the solidification time is significantly over-predicted, which implies that a separate calibration is necessary for this process. Correct prediction and understanding of the heat transfer processes occurring during melting and solidification are necessary for the development of heat transfer elements that reduce charging and discharging times and, thereby lead to thermal storage modules that are practical for residential use.

Acknowledgements

The authors gratefully acknowledge the financial support provided by the Natural Sciences and Engineering Council of Canada (NSERC) and by the University of Western Ontario through the Carbon Solutions program.

References

[1] I. Sarbu and C. Sebarchievici, "Thermal Energy Storage," *Solar Heating and Cooling Systems*, pp. 99–138, Jan. 2017, doi: 10.1016/B978-0-12-811662-3.00004-9.

[2] G. Alva, Y. in, and G. Fang, "An overview of thermal energy storage systems," *Energy*, vol. 144. Elsevier Ltd, pp. 341–378, Feb. 01, 2018. doi: 10.1016/j.energy.2017.12.037.

[3] F. L. Tan, "Constrained and unconstrained melting inside a sphere," *International Communications in Heat and Mass Transfer*, vol. 35, no. 4, pp. 466–475, 2008, doi: 10.1016/j.icheatmasstransfer.2007.09.008.

[4] S. Jevnikar and K. Siddiqui, “Investigation of the influence of heat source orientation on the transient flow behavior during PCM melting using particle image velocimetry,” *J. Energy Storage*, vol. 25, 2019, doi: 10.1016/j.est.2019.100825.
[5] C. W. Chan and F. L. Tan, “Solidification inside a sphere - An experimental study,” *Int. Comm. in Heat and Mass Transfer*, vol. 33, no. 3, pp. 335–341, 2006, doi: 10.1016/j.icheatmasstransfer.2005.10.010.
[6] D. Ghosh and C. Guha, “Numerical and experimental investigation of paraffin wax melting in spherical cavity,” *Int. J. Heat Mass Transf.*, vol. 55, 2019, 1427–1437.
[7] M. Ismail, A. H. Alkhazaleh, J. Masri, A. Masoud Ali, and M. Ali, “Experimental and numerical analysis of paraffin waxes during solidification inside spherical capsules,” *Therm. Sci. Eng. Prog.*, vol. 26, 2021, 101095.
[8] K. Teather and K. Siddiqui, “An Experimental Investigation of Constrained Melting of a Phase Change Material (PCM) in Circular Geometries, Part I: Velocity Characterization,” *J. Energy Storage*, vol. 86 (part A), 2024, 111516.
[9] K. Teather and K. Siddiqui, “An Experimental Investigation of Constrained Melting of a Phase Change Material (PCM) in Circular Geometries, Part II: Temperature Characterization,” *J. Energy Storage*, vol. 86 (part A), 2024, 110206.
[10] “COMSOL Multiphysics Reference Manual,” 1998. [Online]. Available: www.comsol.com/blogs
[11] “ANSYS FLUENT 12.0 User’s Guide,” ANSYS, Inc. Accessed: Nov. 11, 2023. [Online].
[12] V. Antony Aroul Raj, C. Hariharan, R. Velraj, and R. V. Seeniraj, “Numerical Investigations of Outward Solidification in Cylindrical CM Storage Unit,” *Applied Mechanics and Materials*, vol. 787, pp. 177–181, 2015, doi: 10.4028/www.scientific.net/amm.787.177
[13] A. Abderrahmane, N.A.A Qasem, A. Mourad, M. Al-Khaleel, Z. Said, K. Guedri, O. Younis, R. Marzouki, “Enhancing the Melting process of Shell-and-Tube PCM Thermal Energy Storage Unit Using Modified Tube Design,” *Nanomaterials*, vol. 12, no. 17, 2022, doi: 10.3390/nano12173078.124
[14] S. Mat, A. A. Al-Abidi, K. Sopian, M. Y. Sulaiman, and A. T. Mohammad, “Enhanced heat transfer for CM melting in triplex tube with internal-external fins,” *Energy Convers Manag*, vol. 74, pp. 223–236, 2013, doi: 10.1016/j.enconman.2013.05.003.
[15] L. Crnjac, “An investigation of heat transfer enhancement in a thermal storage module,” MESc Thesis, Western University, 2023.
[16] Hemmat, K. Teather, K. Siddiqui, A. G. Straatman, “An Investigation into Computational Modelling of Phase Change Materials using the Enthalpy-Porosity Approach,” Accepted in *Int. J. Num. Meth. For Heat and Fluid Flow*, 2025.